HHS Public Access

Author manuscript

Angew Chem Int Ed Engl. Author manuscript; available in PMC 2017 April 25.

Published in final edited form as:

Angew Chem Int Ed Engl. 2016 April 25; 55(18): 5477–5482. doi:10.1002/anie.201510748.

A Smart Photosensitizer-MnO_2 Nanosystem for Enhanced Photodynamic Therapy via Reducing Glutathione Levels in Cancer Cells

Huanhuan Fan, **Guobei Yan**, **Dr. Zilong Zhao**, **Dr. Xiaoxiao Hu**, **Wenhan Zhang**, **Hui Liu**, **Xiaoyi Fu**, **Ting Fu**, **Prof. Xiao-Bing Zhang**[*], and **Prof. Weihong Tan**[*]

Molecular Science and Biomedicine Laboratory, State Key Laboratory of Chemo/Bio-Sensing and Chemometrics, College of Chemistry and Chemical Engineering, College of Biology, Collaborative Innovation Center for Chemistry and Molecular Medicine, Hunan University, Changsha, 410082, China

Abstract

Photodynamic therapy (PDT) has been applied in cancer treatment by utilizing reactive oxygen species to kill cancer cells. However, a high concentration of Glutathione (GSH) is present in cancer cells and can consume reactive oxygen species. To address this problem, we report the development of a photosensitizer-MnO_2 nanosystem for highly efficient PDT. In our design, MnO_2 nanosheets adsorb photosensitizer chlorin e6 (Ce6), protect it from self-destruction upon light irradiation, and efficiently deliver it into cells. The nanosystem also inhibits extracellular singlet oxygen generation by Ce6, leading to fewer side effects. Once endocytosed, the MnO_2 nanosheets are reduced by intracellular GSH. As a result, the nanosystem is disintegrated, simultaneously releasing Ce6 and decreasing the level of GSH for highly efficient PDT. Moreover, fluorescence recovery, accompanied by the dissolution of MnO_2 nanosheets, can provide a fluorescence signal for monitoring the efficacy of delivery.

Keywords

Glutathione; MnO_2 nanosheet; Singlet oxygen; Cancer cell; Enhanced photodynamic therapy

Photodynamic therapy (PDT) is a clinical cancer treatment method which utilizes reactive oxygen species, such as singlet oxygen ($^1O_2$) generated through the reaction between a photosensitizer and tissue oxygen under illumination, to kill cancer cells. In comparison with traditional cancer therapy methods, such as surgery, chemotherapy and radiotherapy, PDT possesses several unique advantages, including minimal invasion, fewer side effects, negligible drug resistance, and low minimal toxicity.[1-3] As a consequence, quite a few PDT agents (photosensitizers) which possess high $^1O_2$ quantum yields with excellent photophysical properties and good biocompatibility have been discovered for cancer treatment.[4-8] In parallel, the search for strategies enabling efficient delivery of

[*] xbzhang@hnu.edu.cn, tan@chem.ufl.edu.

Supporting information for this article is given via a link at the end of the document.

photosensitizers into cancer cells is ongoing. One efficient approach employs nanocarriers to deliver cancer treatment agents into cancer cells.[9-15] In the past two decades, different nanomaterials, such as metallic, carbon, silica, and organic polymer nanomaterials, have been developed for intracellular photosensitizer delivery.[16-22] Glutathione (GSH) is an important antioxidant and the most abundant low-molecular weight thiol in vivo, with a concentration range from 1 to 15 mM.[23] At the same time, however, it has been shown to consume $^1O_2$ generated by PDT agents, thus greatly reducing the efficiency of PDT and limiting the clinical applications of current PDT agents.[24-26] Therefore, the development of a multifunctional nanosystem which can both enhance the cellular uptake of photosensitizers and decrease the level of GSH in cancer cells in situ is highly desired.

MnO_2 nanosheets, ultrathin semiconductors, have attracted extensive attention in bioanalysis, cell imaging and drug delivery.[27-31] They exhibit several unique features favorable for the delivery of photosensitizers with enhanced PDT efficiency. First, MnO_2 nanosheets can strongly adsorb small organic molecules, such as photosensitizers, via electrostatic interaction and Mn-N coordinate bonds, which can facilitate their endocytosis for intracellular PDT.[28] Second, MnO_2 nanosheets have an intense and broad optical absorption spectrum (~200-600 nm), making them an efficient broad-spectrum fluorescence quencher for the design of fluorescence turn-on probes for monitoring delivery efficiency. Most importantly, MnO_2 nanosheets can react with intracellular glutathione (GSH), resulting in the disintegration of the nanosheets and, hence, complete release of photosensitizers for PDT. This effectively depletes GSH, reducing its effects on $^1O_2$ and enhancing PDT efficiency. Therefore, MnO_2 nanosheets provide a potent and smart nanocarrier for both intracellular delivery of PDT agents and the reduction of intracellular GSH level to improve PDT efficiency.

Herein, we report a photosensitizer-MnO_2 nanosystem assembled by the physisorption of the commonly used photosensitizer chlorin e6 (Ce6) on MnO_2 nanosheets for highly efficient PDT,[32-34] as shown in Scheme 1. In this design, MnO_2 nanosheets act as a nanocarrier for Ce6 and as an oxidant to reduce the level of intracellular GSH. Moreover, they were shown to efficiently quench the fluorescence of Ce6 to provide a turn-on fluorescence signal for monitoring delivery efficiency. In the Ce6-MnO_2 nanosystem, Ce6 is protected by MnO_2 from self-destruction upon light irradiation and can be efficiently delivered into cytoplasm. The nanosystem presents a low fluorescence signal and low phototoxicity in the circulatory system. However, once endocytosed, the MnO_2 nanosheets are reduced by intracellular GSH. As a result, the nanosystem is disintegrated, simultaneously releasing Ce6 and decreasing the level of GSH for highly efficient PDT. Meanwhile, fluorescence recovery, accompanied by the dissolution of MnO_2 nanosheets, provides a reporting signal for monitoring delivery efficiency.

It has been hypothesized that GSH can reduce PDT efficacy. To test this idea, we investigated the inhibitory effect of GSH on $^1O_2$ in buffer. Singlet oxygen sensor green (SOSG) was employed to evaluate the $^1O_2$ generated by several photosensitizers with different $^1O_2$ quantum yields mixed with GSH and SOSG and then irradiated. As shown in Figure S1, 10 mM GSH could efficiently deplete the $^1O_2$ generated by 1 μM Ce6, 20 μM NIR 820 or 100 μM Hematoporphyrin, demonstrating that GSH can easily deplete $^1O_2$ and,

as a result, reduce PDT efficacy.[35] In addition, other biomolecules were mixed separately with Ce6 and then irradiated. As shown in Figure S2, the introduction of these biomolecules induced negligible fluorescence intensity change of Ce6-incubated SOSG under irradiation, indicating that the consumption of $^1O_2$ by GSH is highly specific in living systems.

To construct the Ce6-MnO_2 nanosystem, MnO_2 nanosheets were prepared by ultrasonicating bulk MnO_2,[31] synthesized using H_2O_2 to oxidize $MnCl_2$ in the presence of tetramethylammonium hydroxide and identified by X-ray photoelectron spectroscopy and UV-vis absorption with a peak centered at 360 nm (Figure S3). The results from scanning electron microscopy and transmission electron microscopy indicated that as-prepared MnO_2 presented a sheeted structure. Next, we investigated the adsorption capacity of as-prepared MnO_2 nanosheets for Ce6 photosensitizer by fluorescence analysis based on the excellent fluorescence quenching ability of MnO_2 nanosheets. As shown in Figure S4, different concentrations of MnO_2 nanosheets were mixed with 5 μM Ce6. MnO_2 nanosheets exhibited high quenching efficacy on Ce6. Fluorescence from Ce6 was completely quenched when the concentration of MnO_2 nanosheets was increased to 41.76 μg/mL. At that concentration, the amount of adsorbed Ce6 on 1 μg of as-prepared MnO_2 nanosheets was calculated to be about 120 nmol, demonstrating high Ce6 loading efficiency. Following formation of the Ce6-MnO_2 nanosystem, $^1O_2$ generation from Ce6 was then investigated. As shown in Figure S5, the Ce6-MnO_2 nanosystem presented much lower SOSG fluorescence intensity than that of free Ce6, demonstrating that MnO_2 nanosheets could efficiently inhibit SOG from Ce6 outside the cells and, hence, limit the side effects of PDT.[36]

The Ce6-MnO_2 nanosystem was then mixed with different concentrations of GSH to assess its ability to decompose the nanosystem. As shown in Figure S6, the UV-vis absorption band of MnO_2 nanosheets gradually decreased until it disappeared when the concentration of GSH increased from 0 mM to 10 mM, indicating that MnO_2 nanosheets were reduced to Mn^{2+} ions by GSH. GSH-activated SOG from Ce6 was then investigated. As shown in Figure S7a, with increasing GSH concentration, fluorescence from SOSG was enhanced accordingly, indicating that Ce6 was released as MnO_2 nanosheets were decomposed. However, when the concentration of GSH was larger than 4 mM, fluorescence from SOSG decreased dramatically, as excess GSH could consume $^1O_2$ via reduction, in good agreement with the results in Figure S1. We then increased the concentration of MnO_2 to 522 μg/mL and tested the effect of 10 mM GSH on SOG. As shown in Figure S7b, fluorescence intensity from SOSG increased greatly, indicating that plentiful MnO_2 could enhance PDT efficiency of Ce6 by decreasing the level of GSH.

The delivery efficacy of MnO_2 nanosheets was examined by comparing the internalization of the Ce6-MnO_2 nanosystem with that of free Ce6 in MCF-7 breast cancer cells. As shown by flow cytometry (Figure 1), MCF-7 cells treated with the Ce6-MnO_2 nanosystem showed significantly higher fluorescence intensity than those treated with free Ce6, indicating that the MnO_2 nanosheets could enhance the cellular uptake of Ce6 and release it efficiently. In addition, confocal laser scanning microscopy analysis of cells treated with the Ce6-MnO_2 nanosystem also presented much stronger fluorescence signals in cytoplasm than those treated with free Ce6, in good agreement with the results of flow cytometry. These results also demonstrated the Ce6-MnO_2 nanosystem was mainly distributed in the cytoplasm, and

MnO_2 nanosheets were mainly reduced by the GSH in the cytoplasm. These data suggest that the MnO_2 nanosheets can efficiently deliver photosensitizer Ce6 into cells for photodynamic therapy.

To identify the phototoxicity of the Ce6-MnO_2 nanosystem, MTS assay (MTS=3-(4, 5-dimethylthiazol-2-yl)-5-(3-carboxymethoxyphenyl)-2-(4-sulfophenyl)-2H-tetrazolium) was conducted for the nanosystem with and without irradiation with light. As shown in Figure 2a, cell viability gradually decreased with increasing concentration of Ce6 under irradiation. A nanosystem containing 5 μM of Ce6 could induce 95% of cell death. Without irradiation, however, only negligible cell death was observed with the nanosystem, indicating that the therapeutic effect was highly light-dependent. Moreover, MnO_2 nanosheets were found to have low cytotoxicity with concentration < 60 μg/mL (Figure S9). In Figure 2b, MCF-7 cells were treated with free Ce6 and Ce6-MnO_2 nanosystem with Ce6 at different concentrations, followed by irradiation. With the same concentration of Ce6, free Ce6 showed minimal efficiency for PDT, while the Ce6-MnO_2 nanosystem was much more efficient. These results further demonstrated that MnO_2 nanocarriers could enhance the Ce6 uptake and result in the remarkably increased PDT efficacy.

Next, to investigate PDT efficacy of the Ce6-MnO_2 nanosystem in live cells, the fluorescence and morphological changes of MCF-7 cells pretreated with Ce6-MnO_2 nanosystem and 405 nm laser irradiation (2 mW) were tracked in real time by confocal fluorescence imaging. After treatment with free Ce6 or Ce6-MnO_2 nanosystem for 4 h, the cells were irradiated using the confocal microscope. Upon irradiation, cytoplasmic fluorescence gradually decreased in the first 2 minutes with no significant morphological changes observed for the cells. After 3 minutes irradiation, more and more bubbles appeared on the surface of cells, and the outer membrane was ruptured, but with little observable fluorescence signal, indicating obvious cell death (Figure 2c).[37] In contrast, fluorescence and morphological changes of untreated cells, as shown in Figure S8, were not observed under irradiation, demonstrating that the cell death in Figure 3c was induced by Ce6-based PDT, rather than by the laser only.

To test the effect of GSH on PDT efficiency in cancer cells, we first used commercial agents to regulate the level of GSH.[31] Before incubating with Ce6 or the Ce6-MnO_2 nanosystem, MCF-7 cells were treated with α-lipoic acid (LPA, a GSH synthesis enhancer: 500 μM) for 24 h or N-methylmaleimide (NMM, a GSH scavenger: 2 μM) for 20 min. The cells were then incubated with free Ce6 and Ce6-MnO_2 containing different concentrations of Ce6. In parallel experiments, as shown in Figure S10, we observed an absorbance enhancement at 490 nm for MCF-7 cells treated with LPA, while a distinct decrease of absorbance was observed when MCF-7 cells were treated with NMM. Taken together, these results strongly support the influence of intracellular GSH on PDT.

To identify whether MnO_2 nanosheets have the capacity to improve the efficiency of PDT than other nanomaterials, graphene oxide (GO), which presents a sheeted structure like MnO_2 nanosheets, and mesoporous silica nanoparticles (MSN), which have high payload capacity, were introduced as controls (Figure S11). As shown in Figure 3, cells were treated with Ce6-GO and Ce6-MSN nanosystems with Ce6 at different concentrations. Both Ce6-

GO and Ce6-MSN showed low PDT efficiency. Especially, when the concentration of Ce6 was increased to 5 μM, Ce6-GO and Ce6-MSN induced only 36% and 21% of cell death, respectively, while Ce6-MnO_2 induced 95% of cell death (Figure 2b). These results demonstrated that Ce6-MnO_2 was much more efficient for PDT than other nanocarriers, which might be the synergistic effects of both high Ce6 release efficacy and MnO_2-induced GSH oxidation in cells. Since MnO_2 nanosheets could be reduced by intracellular GSH while GO and MSN could not, leading to the faster release of Ce6 on MnO_2 nanosheets than that of GO and MSN. Moreover, the self-quenching of Ce6 in them will result in poor PDT efficiency.

To further verify the effect of MnO_2-induced GSH oxidation on the PDT efficacy of the nanosystem, free Ce6 at different concentrations and Ce6-MnO_2 nanosystem were incubated with cells separately. As shown in Figure 3c, the fluorescence intensity of cells treated with Ce6-MnO_2 nanosystem containing 1 μM of Ce6 is equal to that treated with 2 μM free Ce6, indicating that the amount of Ce6 released into the cells was about the same for these two treatments. Free Ce6 and Ce6-MnO_2 nanosystem with a 2:1 Ce6 concentration were then employed for further experiments. Figure S12 shows that under the same intracellular Ce6 concentration, Ce6-MnO_2 exhibited much higher PDT efficiency than that of free Ce6. This result together with the low cytotoxicity of free MnO_2 nanosheets (with concentration < 60 μg/mL) indicated that the MnO_2-induced GSH oxidation could remarkable increase the efficiency of PDT.

Then we compared the cytotoxicity of the Ce6-MnO_2 nanosystem with that of free Ce6 at different concentrations. As shown in Figure 3d, PDT efficiency of the Ce6-MnO_2 nanosystem containing 2 μM Ce6 was nearly the same as that of 8 μM free Ce6. However, the fluorescence intensities of cells treated with the Ce6-MnO_2 nanosystem was much weaker than that of cells treated with 8 μM free Ce6, as shown in Figure S13, proving that MnO_2 nanosheets play both a nanocarrier and a GSH scavenger role in Ce6-MnO_2-induced phototoxicity.

To demonstrate the universality of the Ce6-MnO_2 nanosystem, PDT efficiency of the nanosystem was further evaluated for various types of cells, such as HepG2 (liver cancer), HeLa (cervical cancer), A549 (lung cancer), MCF-7 (breast cancer) and 293T (Human embryonic kidney) cells. As shown in Figure S14a, this nanosystem exhibited high PDT efficacy for all cell lines, with a slightly lower efficacy for HepG2 cells and slightly higher efficacy for 293T cells. This difference may have resulted from the different GSH levels in these cell lines. To verify this hypothesis, we further investigated intracellular GSH levels in different cell lines using confocal microscopy based on GSH-activated fluorescence recovery of Ce6, treating all cells with the Ce6-MnO_2 nanosystem at the same concentration (Figure S14b). The amount of the nanosystem present in cells was first analyzed by inductively coupled plasma optical emission spectrometry (ICP-OES). Experimental results in Figure S15a indicate that the same level of MnO_2 nanosheets was uptaken by different types of cells. Cancer cells, especially HepG2 cells, treated with the Ce6-MnO_2 nanosystem presented higher fluorescence signals than those of 293T cells, indicating a higher GSH level in cancer cells than in normal cells. In addition, since the diameter of MCF-7 cells was about 25 μm (Figure S15b), the average concentration of MnO_2 in MCF-7 cells was

calculated to be about 2.53 mM based on the result of ICP-OES. The local concentration of MnO_2 in cells would be much higher than 2.53 mM, which is sufficient to reduce intracellular GSH concentration. Taken together, these results indicate that the Ce6-MnO_2 nanosystem has broad applicability for killing different cell lines with PDT.

The feasibility of *in vivo* PDT applications of the nanosystem was then verified by investigating the fate of Ce6 and Ce6-MnO_2 nanosystem using fluorescence imaging assay. Athymic nude mice with subcutaneous ZR-75-30 breast cancer xenografts were selected as the animal model. Ce6-MnO_2 nanosystem-treated ZR-75-30 cells resulted in apoptosis, as shown in Figure S16 and S17. When the size of tumors reached ~ 60 mm^3, the mice were intratumorally injected with 40 μL of Ce6 or 50 μL of Ce6-MnO_2 nanosystem, both containing 100 μM of Ce6. As shown in Figure S18a and S18b, after intratumoral injection, fluorescence intensity of Ce6 in free Ce6-loaded tumors decreased gradually, while that in the Ce6-MnO_2-loaded tumors increased in the first hour and then decreased gradually. To explain these results, MnO_2 nanosheets were reduced gradually by intracellular GSH in the first hour, accounting for the recovery of Ce6 fluorescence. The decreased fluorescence most likely resulted from the spread of Ce6 throughout the animal's body. Thus, the best timing for PDT is 1 hour after intratumoral injection.

In vivo therapeutic efficacy of Ce6, MnO_2 nanosheets and the Ce6-MnO_2 nanosystem was assessed by monitoring the growth rate of tumors. The sizes of tumors were normalized to their initial values.[38] Experimental results indicated that the free Ce6 and Ce6-MnO_2 nanosystem groups with light irradiation showed either remarkable delay in tumor growth or observable tumor regression compared with the control group treated with MnO_2 nanosheets after two weeks (Figure 4a). In contrast, the groups without light irradiation showed no apparent change of tumor size compared with the control group, indicating that the therapeutic effect was highly light-dependent. It is noteworthy that the Ce6-MnO_2 nanosystem-treated group exhibited higher therapeutic efficacy compared with that of the free Ce6- or MnO_2 nanosheets-treated groups on day 12. The weights of these mice in different groups in Figure 4b were in good agreement with the results of the growth rate of tumors. These results clearly demonstrated that enhanced PDT was achieved for the Ce6-MnO_2 nanosystem, which should be the results that Ce6-MnO_2 nanosystem could both enhance Ce6 uptake in cells (need lower dose injection of PDT agent to decrease its side effect), and reduce GSH Levels in cells due to MnO_2-induced GSH oxidation. H&E staining of tumor sections was performed on day 12, and the results are shown in Figure 4c. In PBS, histological sections of the MnO_2- and Ce6-treated groups showed infiltrating tumor cells with highly pleomorphic nuclei and many mitoses, indicating limited benefit from laser treatment. These results indicate that the Ce6-MnO_2 nanosystem has excellent theranostic capability without noticeable toxicity and that it is suitable for imaging-guided PDT of tumors *in vivo*.

In summary, we have developed a smart photosensitizer-MnO_2 nanosystem with both high intracellular delivery efficiency and enhanced photodynamic therapy efficacy by reducing glutathione levels in cancer cells. This Ce6-MnO_2 nanosystem exhibits: (i) high Ce6 loading efficiency on MnO_2 nanosheets, (ii) enhanced delivery of Ce6 into cells, and (iii) simultaneous release of Ce6 and decrease of GSH level for highly efficient PDT. The

multifunctional MnO_2 nanosheets also show good biocompatibility, thus facilitating their biomedical applications, particularly for cancer theranostics. Therefore, this smart Ce6-MnO_2 nanosystem shows high promise as a future multifunctional treatment tool for simultaneous therapy and monitoring for various types of cancers.

Supplementary Material

Refer to Web version on PubMed Central for supplementary material.

Acknowledgements

This work was supported by the National Key Scientific Program of China (2011CB911000), the National Key Basic Research Program of China (No. 2013CB932702), NSFC (Grants 21325520, 21327009, 21405041, J1210040, 21177036), the Foundation for Innovative Research Groups of NSFC (Grant 21521063), the National Instrumentation Program (2011YQ030124).

References

1. Lovell JF, Liu TW, Chen J, Zheng G. Chem. Rev. 2010; 110:2839–2857. [PubMed: 20104890]
2. Celli JP, Spring BQ, Rizvi I, Evans CL, Samkoe KS, Verma S, Pogue BW, Hasan T. Chem. Rev. 2010; 110:2795–2838. [PubMed: 20353192]
3. Dolmans DE, Fukumura D, Jain RK. Nat. Rev. Cancer. 2003; 3:380–387. [PubMed: 12724736]
4. Na JI, Kim SY, Kim JH, Youn SW, Huh CH, Park KC. Laser surg. Med. 2011; 43:200–205.
5. Zhang Y, Zhang N, Tang ZR, Xu YJ. ACS nano. 2012; 6:9777–9789. [PubMed: 23106763]
6. Ahn JC. Gen. Physiol. Biophys. 2013; 32:405–413. [PubMed: 23846258]
7. Lei K, Tan S, Du W, Xu Y, Lin S, Zheng Y, Zou F, Xu Y, Liu J. Tumor Biol. 2015; 1:1–10.
8. Liang R, Tian R, Ma L, Zhang L, Hu Y, Wang J, Wei M, Yan D, Evans DG, Duan X. Adv. Funct. Mater. 2014; 24:3144–3151.
9. Slowing II, Vivero-Escoto JL, Wu CW, Lin VSY. Adv. Drug Delivery Rev. 2008; 60:1278–1288.
10. Sun C, Lee JS, Zhang M. Adv. Drug Delivery Rev. 2008; 60:1252–1265.
11. Liong M, Lu J, Kovochich M, Xia T, Ruehm SG, Nel AE, Tamanoi F, Zink JI. ACS nano. 2008; 2:889–896. [PubMed: 19206485]
12. Panyam J, Labhasetwar V. Adv. Drug Delivery Rev. 2003; 55:329–347.
13. Gao J, Gu H, Xu B. Acc. Chem. Res. 2009; 42:1097–1107. [PubMed: 19476332]
14. Della Rocca J, Liu D, Lin W. Acc. Chem. Res. 2011; 44:957–968. [PubMed: 21648429]
15. Al-Jamal WT, Kostarelos K. Acc. Chem. Res. 2011; 44:1094–1104.
16. Roy I, Ohulchanskyy TY, Pudavar HE, Bergey EJ, Oseroff AR, Morgan J, Dougherty TJ, Prasad PN. J. Am. Chem. Soc. 2003; 125:7860–7865. [PubMed: 12823004]
17. Bechet D, Couleaud P, Frochot C, Viriot ML, Guillemin F, Barberi-Heyob M. Trends Biotechnol. 2008; 26:612–621. [PubMed: 18804298]
18. van Nostrum CF. Adv. Drug Delivery Rev. 2004; 56:9–16.
19. Wieder ME, Hone DC, Cook MJ, Handsley MM, Gavrilovic J, Russell DA. Photochem. Photobiol. Sci. 2006; 5:727–734. [PubMed: 16886087]
20. Ohulchanskyy TY, Roy I, Goswami LN, Chen Y, Bergey EJ, Pandey RK, Oseroff AR, Prasad PN. Nano Lett. 2007; 7:2835–2842. [PubMed: 17718587]
21. Nishiyama N, Morimoto Y, Jang WD, Kataoka K. Adv. Drug Delivery Rev. 2009; 61:327–338.
22. Cheng Y, Samia AC, Meyers JD, Panagopoulos I, Fei B, Burda C. J. Am. Chem. Soc. 2008; 130:10643–10647. [PubMed: 18642918]
23. Zhang X, Wu FG, Liu P, Gu N, Chen Z. Small. 2014; 10:5170–5177. [PubMed: 25111498]
24. Jiang F, Robin A, Katakowski M, Tong L, Espiritu M, Singh G, Chopp M. Lasers med. Sci. 2003; 18:128–133. [PubMed: 14505195]

25. Kiesslich T, Plaetzer K, Oberdanner CB, Berlanda J, Obermair FJ, Krammer B. FEBS Lett. 2005; 579:185–190. [PubMed: 15620711]
26. Henderson BW, Miller AC. Radiat. Res. 1986; 108:196–205. [PubMed: 3097749]
27. Zhao Z, Fan H, Zhou G, Bai H, Liang H, Wang R, Zhang X, Tan W. J. Am. Chem. Soc. 2014; 136:11220–11223. [PubMed: 25061849]
28. Chen Y, Ye D, Wu M, Chen H, Zhang L, Shi J, Wang L. Adv. Mater. 2014; 26:7019–7026. [PubMed: 25156250]
29. Yuan Y, Wu S, Shu F, Liu Z. Chem. Commun. 2014; 50:1095–1097.
30. Meng HM, Jin Z, Lv Y, Yang C, Zhang XB, Tan W, Yu RQ. Anal. Chem. 2014; 86:12321–12326. [PubMed: 25399841]
31. Deng R, Xie X, Vendrell M, Chang YT, Liu X. J. Am. Chem. Soc. 2011; 133:20168–20171. [PubMed: 22107163]
32. Avula U, Yoon H, Lee C, Kaur k. Rafael J, Takemoto Y, Ennis S, Morady F, Herron T, Berenfeld O, Kopelman R, Kalifa J. Sci. Transl. Med. 2015; 311:172–172.
33. Xu Y, He R, Lin D, Ji M, Chen J. nanoscale. 2015; 7:2433–2441. [PubMed: 25565649]
34. Wang Z, Ma R, Yan L, Chen X, Zhu G. Chem. Commun. 2015; 51:11587–11590.
35. Jones C, Lawrence A, Wardman P, Burkitt M. Biochem. Soc. Trans. 2003; 31:1337–1340. [PubMed: 14641058]
36. Zhu Z, Tang Z, Phillips JA, Yang R, Wang H, Tan W. J. Am. Chem. Soc. 2008; 130:10856–10857. [PubMed: 18661988]
37. Tian J, Ding L, Ju H, Yang Y, Li X, Shen Z, Zhu Z, Yu JS, Yang CJ. Angew. Chem. Int. Ed. 2014; 53:9544–9549.
38. Lin J, Wang S, Huang P, Wang Z, Chen S, Niu G, Li W, He J, Cui D, Lu G. ACS nano. 2013; 7:5320–5329. [PubMed: 23721576]

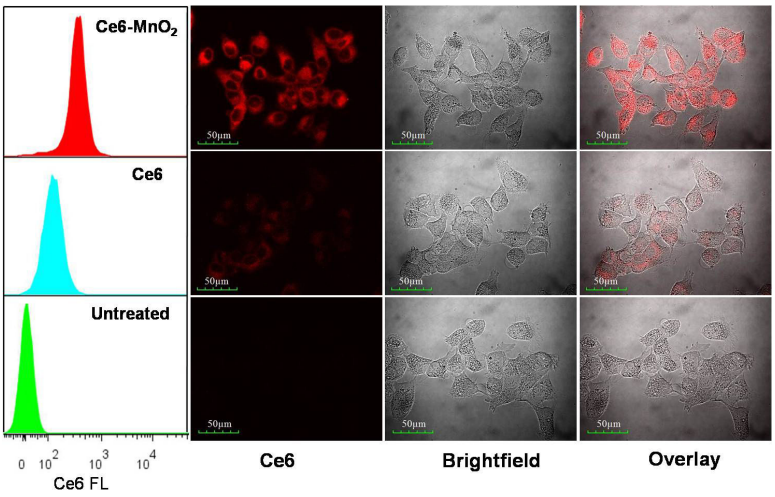

Scheme 1.

Activation mechanism of the Ce6-MnO_2 nanosystem for highly efficient photodynamic therapy. The nanosheet can adsorb and efficiently deliver photosensitizers into cells and protect them from self-destruction upon light irradiation. Once endocytosed, the nanosystem is disintegrated upon reduction of MnO_2 nanosheets by intracellular GSH, simultaneously releasing Ce6 for fluorescence imaging and decreasing the level of GSH for highly efficient PDT.

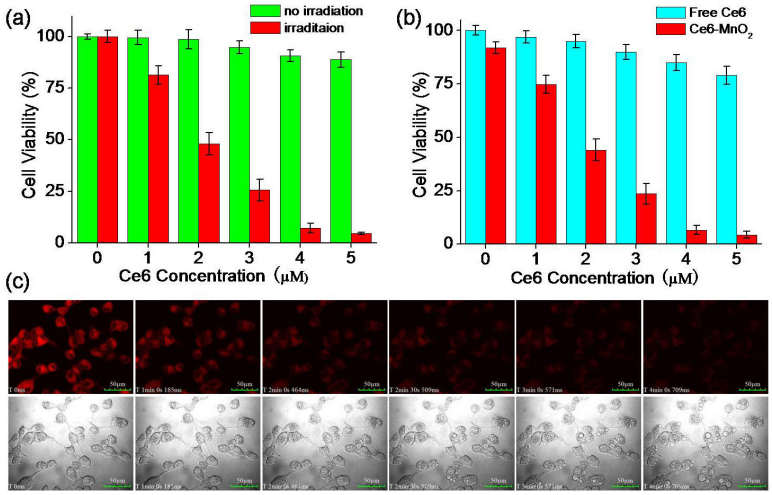

Figure 1.

Flow cytometry analysis (left) and confocal fluorescence images (right) of MCF-7 cells treated with free Ce6 and Ce6-MnO_2 nanosystem. Concentrations of Ce6 and MnO_2 nanosheets were 1 μM and 41.76 μg/mL, respectively.

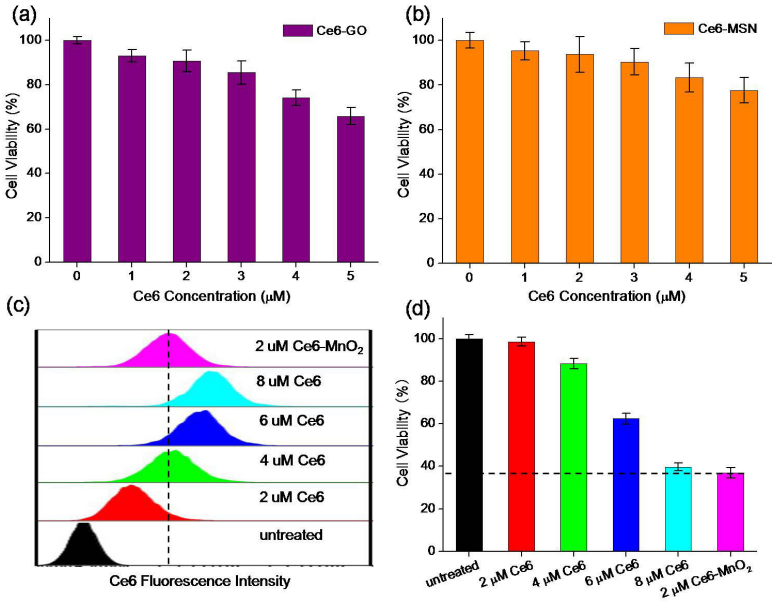

Figure 2.

(a) Cytotoxicity of Ce6-MnO_2 nanosystem with Ce6 at different concentrations in the presence or absence of irradiation. (b) Phototoxicity of free Ce6 and Ce6-MnO_2 nanosystem with Ce6 at different concentrations. (c) Real-time fluorescence images and morphology of MCF-7 cells treated with Ce6-MnO_2 nanosystem and laser at 405 nm (top) and bright-field images (bottom). Concentration of MnO_2 nanosheets in these studies was 41.76 μg/mL.

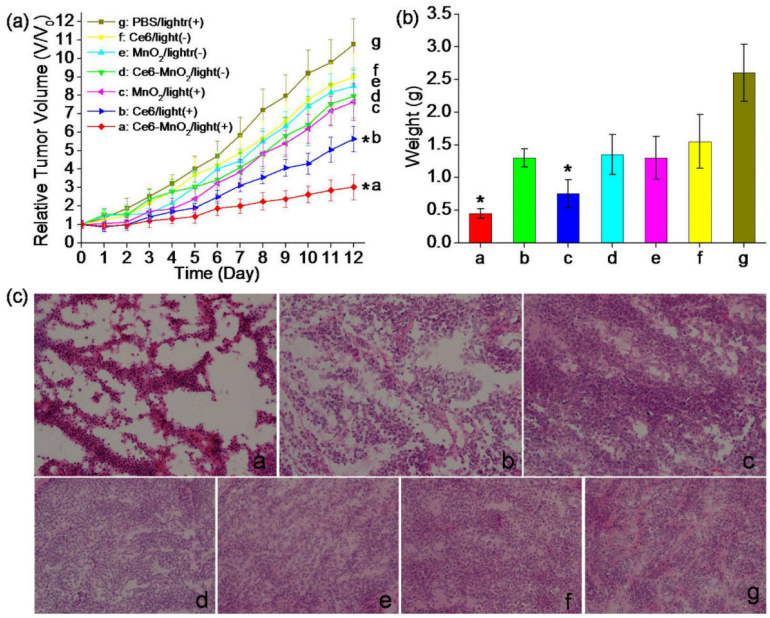

Figure 3.

Phototoxicity of Ce6-GO (a) and Ce6-MSN (b) nanosystem on MCF-7 cells with Ce6 at different concentrations as indicated. (c) Flow cytometry analysis of MCF-7 cells treated with Ce6-MnO_2 nanosystem and different concentrations of free Ce6. (d) Cytotoxicity of MCF-7 cells treated with Ce6-MnO_2 nanosystem and different concentrations of free Ce6. Concentration of MnO_2 nanosheets in these studies was 41.76 μg/mL.

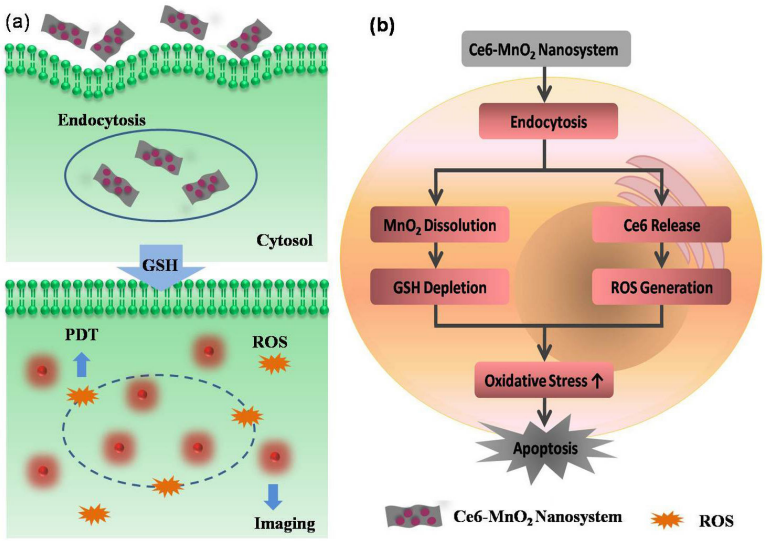

Figure 4.

(a) Tumor growth curves of different groups of tumor-bearing mice after treatment. Tumor volumes were normalized to their initial sizes. Error bars represent the standard deviations of 3 mice per group. Asterisk indicates $P < 0.05$. Weight of tumors (b) and H&E stained tumor sections (c) collected from different groups of mice 12 days post treatment.